

A Novel B5G Frequency Non-Stationary Wireless Channel Model

Yi Tan, Cheng-Xiang Wang, *Fellow, IEEE*, Jesper Ødum Nielsen, Gert F. Pedersen, and Qiuming Zhu, *Member, IEEE*

Abstract—Frequency non-stationarity is an important statistical property for beyond the fifth generation (B5G) wireless communication channels due to extremely large bandwidths used in millimeter wave (mmWave) and terahertz (THz) communications. In this paper, a general averaged power delay profile (APDP) method is first introduced as a metric to determine the stationarity regions of wireless channels in the time, frequency, and spatial domains. Then, we apply this method to determine the frequency stationarity regions (FSRs) of channel measurements in a sub-6 GHz frequency band (2–4 GHz) and two mmWave frequency bands (14–16 GHz and 28–30 GHz). Frequency non-stationary (FnS) properties are found from all of the three bands. A novel FnS channel model is then proposed to model wireless channels in all frequency bands. We first split a FnS channel into a few frequency stationary (FS) sub-band channels and model them one by one, which are finally combined as a FnS channel model considering the cluster evolution in the frequency domain as well as the frequency consistency of sub-band channels. Simulation results show that the frequency correlation functions (FCFs) of the proposed FnS channel model can well fit those of the measured FnS channels.

Index Terms—Frequency stationarity region, general averaged power delay profile method, frequency non-stationary channel model, frequency domain cluster evolution, frequency consistency.

Manuscript received February 13, 2020; revised September 23, 2020; accepted December 29, 2020. Date of current version January 07, 2021. The authors would like to acknowledge gratefully the support of this work from National Key R&D Program of China under Grant 2018YFB1801101, the National Natural Science Foundation of China (NSFC) under Grant 61960206006, the Frontiers Science Center for Mobile Information Communication and Security, the High Level Innovation and Entrepreneurial Research Team Program in Jiangsu, the High Level Innovation and Entrepreneurial Talent Introduction Program in Jiangsu, the Research Fund of National Mobile Communications Research Laboratory, Southeast University, under Grant 2020B01, the Fundamental Research Funds for the Central Universities under Grant 2242020R30001, and the EU H2020 RISE TESTBED2 project under Grant 872172. The authors would also like to express sincere gratitude to Kim Olesen, Kristian Bank, and Wei Fan from Aalborg University for their invaluable work in the channel measurement campaigns.

Y. Tan is with MN SoC RD Beamer L1 IP 3 SG, Nokia Solutions and Networks, Karakaari 7, 02610 Espoo, Finland (email: tan.yi@nokia.com).

C.-X. Wang (corresponding author) is with National Mobile Communications Research Laboratory, School of Information Science and Engineering, Southeast University, Nanjing, 210096, China, and also with Purple Mountain Laboratories, Nanjing, 211111, China (email: chxwang@seu.edu.cn).

J. Ø. Nielsen and G. F. Pedersen are with APMS section, Dept. of Electronic Systems, Technical Faculty of IT and Design, Aalborg University, DK-9220 Aalborg, Denmark (email: {jni, gfp}@es.aau.dk).

Q. Zhu is with the Key Laboratory of Dynamic Cognitive System of Electromagnetic Spectrum Space, College of Electronic and Information Engineering, Nanjing University of Aeronautics and Astronautics, Nanjing 211106, Jiangsu, China (email: zhuqiuming@nuaa.edu.cn).

I. INTRODUCTION

Millimeter wave (mmWave) communication technology is one of the most promising candidates for the fifth generation (5G) and even beyond 5G (B5G) wireless networks [1], [2]. There are about 7 GHz bandwidth resource available at 60 GHz band (unlicensed) and 1 GHz bandwidth resource available at 28 GHz and 38 GHz bands [3]. In current mmWave channel measurements, channel sounding signals with 500 MHz or even broader bandwidths are normally utilized [4]–[7] in the study of 5G channels. Terahertz (THz) technology has been considered as a possible candidate for B5G wireless communication networks, claiming that over 50 GHz bandwidth can be used for various applications, such as ultra fast kiosk downloads, fixed radio links, wireless local area networks (LANs), THz nanocells or inter-chip links [8]. In [9], channel characteristics were investigated at 300 GHz with 20 GHz bandwidth. Due to large bandwidths, the propagation properties of mmWave and THz channels can be very different from those of channels in the third generation (3G) and fourth generation (4G) communication systems.

The stationarity study of wireless channels plays a fundamental role in the analysis of channel measurements and channel modeling. Wide-sense stationary (WSS) channels were introduced in [10], and the stationarity assumptions in the time, frequency, and spatial domains can be found in [11], [12]. In WINNER II/+ [13], [14], ITU-R [15], and 3GPP [16] channel models, the concept of segments and drops were used to define the “quasi-stationary” periods, during which the channels satisfy the WSS assumption. In QuaDRiGa [17], COST 2100 [18], and recently developed channel models based on WINNER+ [19], [20], time evolution was used in the study of channel non-stationarities in the time domain, based on the trajectory of a mobile terminal and birth-death processes. Similarly, time evolution was also used in the modeling of high-speed train (HST) and vehicle-to-vehicle (V2V) channels [21]–[25]. In the study of massive multiple-input and multiple-output (MIMO) channels, it was shown that the cluster powers vary over the large antenna array [26], [27]. The spatial stationarity assumption does not hold for the whole large antenna array. The modeling of spatial-variation over large antenna arrays was suggested for the COST 2100 channel model based on the modification of visibility region (VR) [28]. A recently developed novel massive MIMO channel model in [29] addressed the spatial non-stationarity along the antenna axis. In [30]–[32], birth-death processes were proposed to model both the temporal and spatial non-stationarities of

channels in a similar manner. More related research results can be found in [33].

Regarding the stationarity studies in the frequency domain, there are rich research results related to ultra-wide band (UWB) channels. IEEE 802.15.4a UWB channel model can support up to 2 GHz bandwidths [34]. Due to the fact that the wavelengths of sounding signals used in channel measurements are comparable to the sizes of objects in the environment, the fundamental propagation processes such as reflection and diffraction are frequency dependent within UWB channels [35]. Since the frequency stationarity assumption does not hold for the whole bandwidth, UWB channels can be considered as frequency non-stationary (FnS) channels. In [6], the frequency-selective propagation phenomena of mmWave channels were found. In [36], the results of root mean square (RMS) delay spread (DS) and angle spread (AS) were shown to be frequency dependent within 6 GHz bandwidth, i.e., 2–8 GHz. MmWave channels normally have comparable bandwidths to those of UWB channels. In METIS [37], [38], mmWave channel measurements with 4 GHz bandwidth were used. Map-based mmWave channel models addressed the frequency range up to 100 GHz and the bandwidths of mmWave channels up to 10% of the center frequency can be supported. We can expect that the frequency stationarity assumption does not always hold for mmWave channels within such broad bandwidths. This can happen when utilizing mmWave communications in the environments such as factories, warehouses, mines of coal/metals, chemistry laboratories, etc., where the sizes of objects are comparable to the wavelengths of mmWave signals. In the ray tracing models of mmMAGIC [39], we can also find that the diffuse scattering at mmWave frequencies was studied based on the similar concern that the sizes of objects are comparable to the wavelengths of mmWave signals. However, in the standard mmWave channel models, such as IEEE 802.15.3c [40], IEEE 802.11ad [41], MiWEBA [42], mmMAGIC, METIS, and those mmWave channel models developed recently [5], [43], [44], the channel parameters were normally considered as frequency stationary (FS).

In the development of 5G/B5G channel models, the general studies of frequency dependent channel parameters can be found in 5GCM [45] and latest 3GPP [16] channel models. We can observe the drift of channel parameters within a few consecutive GHz frequency intervals in both sub-6 GHz and mmWave frequency ranges. In the latest 3GPP, IMT 2020 [46], and 5GCM models, a new component was developed to support the simulation of advanced massive MIMO channels with large bandwidths and large antenna arrays. If the bandwidth is greater than the ratio of the speed of light to the maximum antenna aperture, the channel coefficient generation step related to modeling clusters is updated to model individual rays. This implies that the WSS assumption may not hold for the channels with large bandwidths and large antenna arrays. However, that criterion is not suitable to determine the FnS properties and it cannot be used to model the FnS channels. Since broad bandwidth resource is the main merit of using mmWave frequencies in 5G and B5G communications, the studies about the FnS properties of mmWave channels are required.

In this paper, we first introduce a general averaged power delay profile (APDP) method, extended from [47], as a metric to study the stationarities of channels in time, frequency, and spatial domains. We apply it to investigate frequency stationarity regions (FSRs) of channels in both sub-6 GHz and mmWave frequency bands based on real channel measurements, showing the FnS properties of measured channels. Then, a general FnS channel model is proposed to model wireless channels in all frequency bands.

The contributions of this paper are summarized as follows.

- The channel measurements in both sub-6 GHz and mmWave frequency bands were performed in a basement environment. The FSRs of channels in three bands are compared and the FnS properties are found. The variation of statistical parameters within the bandwidth of FnS channels is illustrated. The phenomenon of frequency non-stationarity is shown.
- A novel FnS channel model is proposed to model wireless channels in all frequency bands, including sub-6 GHz and mmWave bands. In the proposed model, a FnS channel is split into a few FS sub-band channels, modeled one by one and then combined into one FnS channel model. Thus, this model also explains the difference between wideband FS and FnS channels.
- For easy implementation, we model the first sub-band channel similar to the 3GPP channel model [16]. The rest sub-band channels are then modeled considering the cluster evolution in the frequency domain. It is worth mentioning that the frequency-domain cluster evolution ensures the frequency consistency of simulated sub-band channels, similar to the consistency studies of simulated channels in temporal and spatial domains in [17] and [50].

The reminder of paper is organized as follows. Section II introduces a general APDP method to estimate the stationarity regions in time, frequency, and spatial domains. The data analysis of frequency stationarity based on real channel measurements is shown in Section III. In Section IV, a FnS channel model is proposed to model the FnS properties of the measured channels in both sub-6 GHz and mmWave frequency bands. The details of generating the FnS channel coefficients can be found in Section V. The validation of the proposed FnS channel model is shown in Section VI. Finally, conclusions are drawn in Section VII.

II. STATIONARITY REGIONS IN TIME, FREQUENCY, AND SPATIAL DOMAINS

The methods, such as the APDP [48] and covariance matrix distance (CMD) [51]–[53], are generally used to estimate the stationarity regions of channels in the time and spatial domains. Though the CMD method can be used to estimate the stationarity region in the frequency domain, the channel correlation based on antenna arrays is required in the calculation. Compared with that, the APDP method does not have such limit. In this section, a more general method based on APDP in [48] is introduced. It can be used to study the stationarities of channels in the time, frequency, and spatial domains.

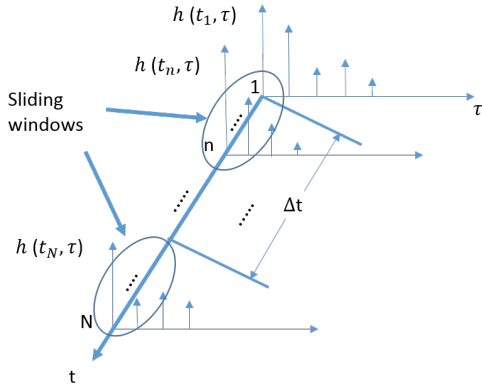


Fig. 1. Sliding windows of APDPs moving along the time axis.

A. General APDP Method Applied in the Time Domain

For a 1×1 wideband wireless channel, we define $h(t_i, \tau)$ as a channel impulse response (CIR). Then the instantaneous power delay profile (PDP) $P_h(t_i, \tau) = |h(t_i, \tau)|^2$ can be seen as a snapshot of the channel at specific time $t_i, i = 1, 2, \dots, N$, and we assume there are N snapshots in total as Fig. 1. We define $\overline{P}_h(t, \tau)$ as

$$\overline{P}_h(t, \tau) = \frac{1}{n} \sum_{i=1}^n |h(t_i, \tau)|^2 \quad (1)$$

to present the average PDP of n -snapshots ($n \ll N$) in one sliding window on the time axis t . Also, let us define $\overline{P}_h(t + \Delta t, \tau)$ as another APDP of n -snapshots as it moves forward along the time axis t with a distance of Δt , where t is the average time of t_i . It can be considered as the middle t_i in the sliding window. The correlation coefficient between the APDPs is defined as

$$c(t, \Delta t) = \frac{\int \overline{P}_h(t, \tau) \overline{P}_h(t + \Delta t, \tau) d\tau}{\max\{\int \overline{P}_h(t, \tau)^2 d\tau, \int \overline{P}_h(t + \Delta t, \tau)^2 d\tau\}}. \quad (2)$$

Based on the correlation coefficient curve, we can determine an allowance of similarity level (ASL) of the channel properties as the threshold (between 0 to 1) [47]. Then the region between the maximum of correlation coefficient to this ASL is considered statistical stationary, i.e. it satisfies the wide sense stationary conditions and it is inside the stationarity region.

Therefore, if the correlation coefficients $c(t, \Delta t)$ between the APDPs are all higher than the ASL tc_{ASL} , then the stationary interval d_t is defined as the stationarity region in the time domain

$$d_t = \max\{\Delta t \mid c(t, \Delta t) \geq tc_{ASL}\}. \quad (3)$$

We assume that the n -snapshots used to calculate the APDPs are within a very small interval that is much smaller than the stationary region. Using the larger value of $\int \overline{P}_h(t, \tau)^2 d\tau$ and $\int \overline{P}_h(t + \Delta t, \tau)^2 d\tau$ in the denominator of (2) is to assure the correlation coefficient is smaller than 1 when using the real measurement data in the calculation. Note that Δt can be both positive and negative.

In practice, if an ensemble of CIRs measured at different time points within a time interval satisfy the WSS assumption,

we consider them to be within one stationarity region [54], and the statistical parameters of the channel in such time interval can be estimated. This is not the same as the coherence time interval within which the CIRs can be considered approximately the same [11]. The ASL is the threshold to determine the size of the stationarity region. We may consider it as the worst tolerable inaccuracy from the systematic level point of view, where the performance of communication systems is predicted based on the simulated wireless channels according to those estimated statistical parameters. However, there is no uniform verdict on the value of ASL at the moment. It can depend on the personal judgement in the data analysis of channel measurements in each individual environment.

B. General APDP Method Applied in the Spatial Domain

The definition of stationarity region in the spatial domain is very similar to that in the time domain. The sliding window moves along spatial axis (along the antenna array) instead of time axis, whilst other procedures maintain the same. For a $N \times 1$ wideband wireless channel scenario, we replace t by r and replace Δt by Δr in (1) to (3).

C. General APDP Method Applied in the Frequency Domain

In Fig. 2, two cluster-maps are used to represent two different FSRs of the same channel (environment). One is at high frequencies and the other is at low frequencies. Within each of the FSR, the statistical parameters of the channel does not change but they are different for the two FSRs. If the bandwidth of a channel is sufficiently large to cover both the FSRs at high frequencies and low frequencies, then such a channel is considered as a FnS channel. For example, the fundamental propagation processes such as reflection and diffraction are frequency-dependent within the bandwidths of UWB channels, because the wavelengths of sounding signals used in channel measurements are comparable to the sizes of objects in the environment [35]. There are also rich studies of frequency-dependent statistical parameters within the bandwidth of UWB channels (including the frequency range below 6 GHz) [34]. This means that UWB channels have covered more than one FSRs. Similar explanation of such phenomenon can be found in [55].

The general APDP method used in estimating the FSRs is an extension of the APDP method [48] used in estimating the stationarity regions in the time and spatial domains.

1) *Case 1: Averaging on Snapshots:* For a 1×1 wideband wireless channel, we define $H(t_i, f)$ as channel transfer function (Fourier transformation of $h(t_i, \tau)$). Then the instantaneous power transfer function (PTF) of the channel $P_H(t_i, f) = |H(t_i, f)|^2$ can also represent a snapshot of the channel at specific time $t_i, i = 1, 2, \dots, N$. We assume there are N snapshots in total as shown in Fig. 3, and the bandwidth of each snapshot consists of M frequency points.

First, we average the PTF of n -snapshots along time axis t as the average PTF (APTF), which can be expressed as

$$\overline{P}_H(t, f) = \frac{1}{n} \sum_{i=1}^n |H(t_i, f)|^2 \quad (4)$$

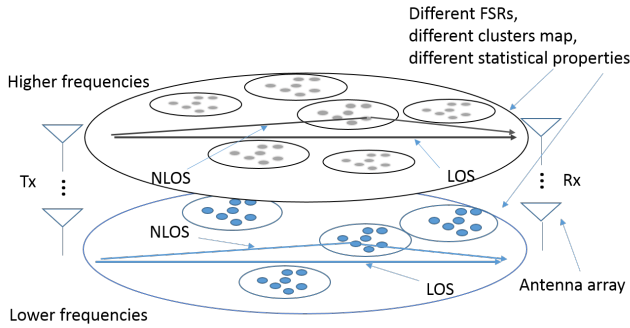


Fig. 2. FSRs of the channel at high frequencies and low frequencies in the same environment.

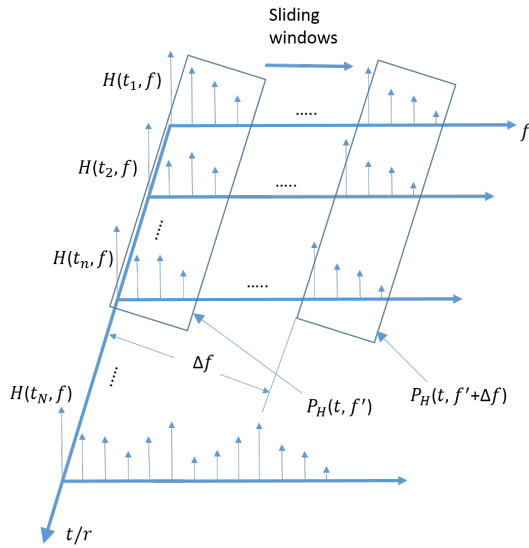


Fig. 3. Sliding-windows of sub-APTFs moving along the frequency axis (we denote $P_H(t, f')$ as the $\overline{P_H}(t, f')$ before averaging).

where t is the average time of t_i . Second, we define m -frequency-points sub-APTF ($m \ll M$) as $\overline{P_H}(t, f')$ in one sliding window on the frequency axis f , and define another m -frequency-points sub-APTF $\overline{P_H}(t, f' + \Delta f)$ as it moves forward along the frequency axis f with a distance of Δf . In order to avoid misunderstanding, we define f' as the frequencies within the sliding-windows. The correlation coefficient between the sub-APTFs is defined as

$$c(f, \Delta f) = \frac{\int \overline{P_H}(t, f') \overline{P_H}(t, f' + \Delta f) df'}{\max\{\int \overline{P_H}(t, f')^2 df', \int \overline{P_H}(t, f' + \Delta f)^2 df'\}}. \quad (5)$$

Similarly, based on the correlation coefficient curve $c(f, \Delta f)$, we can determine an ASL $f_{c_{ASL}}$ of the channel properties as the threshold. The region between the maximum of correlation coefficient to $f_{c_{ASL}}$ is considered statistical stationary and the stationary bandwidth d_f is defined as the FSR in the frequency domain, i.e.,

$$d_f = \max\{\Delta f \mid c(f, \Delta f) \geq f_{c_{ASL}}\}. \quad (6)$$

Likewise, we assume that the sub-APTFs are within a bandwidth that is much smaller than the stationary bandwidth.

Note that the n -snapshots selected in the first step should be within one stationarity region in the time domain. For the sub-APTFs in (5), we can consider them as imaginary FS-CIRs with much narrower bandwidths after Fourier transforming them to the time domain. However, in Section II-A and II-B, the complete CIRs should be used since the transmitted signals in reality can be FnS and it is required to estimate the channel properties based on the FnS sounding signals used in the channel measurement.

2) *Case 2: Averaging on Antenna Array:* For a $N \times 1$ wireless channel scenario, such as using vector network analyzer (VNA) to measure a time-invariant channel environment based on virtual antenna array methodology [56], we calculate PTF based on antenna arrays instead. Here we define $P_H(r_i, f) = |H(r_i, f)|^2$ as the PTF, and r_i is the antenna position along “ r axis” as in Fig. 3. Compared with case 1, the APTF should be denoted as

$$\overline{P_H}(r, f) = \frac{1}{n} \sum_{i=1}^n |H(r_i, f)|^2. \quad (7)$$

The first step is now changed to average the PTFs based on the CIRs measured by an n -antenna subarray. Then the second step and the following are the same.

Similarly, the n -antenna subarray used to calculate the APTF should be selected within one stationarity region in spatial domain.

III. CHANNEL MEASUREMENTS AND DATA ANALYSIS

A. Channel Measurements and Data Processing

The time-invariant channel measurements were performed in a big and empty indoor basement environment, as described in [49]. The channel sounder is consisted of a VNA and a large virtual uniform circular array (UCA) with the radius 0.5 m. The channel was measured at a sub-6 GHz frequency band of 2–4 GHz, and two mmWave frequency bands of 14–16 GHz and 28–30 GHz. There are 750 frequency points within each of the frequency bands (frequency interval is 2.67 MHz). The area of the basement was 7.85 m \times 7.71 m as in Fig. 4. Two bi-conical antennas with a frequency range from 2–30 GHz were used at the transmitter (Tx) and the receiver (Rx). Their radiation patterns are omni-directional on the horizontal plane. One antenna was fixed at about 1 m height at the Tx side. The other one was moved along the trajectory of the virtual UCA at 1 m height at the Rx side. The whole UCA consists of 720 virtual antennas, and the distance between each two adjacent virtual antenna positions was 0.0044 m (less than $\lambda/2$ at 30 GHz). Both line-of-sight (LOS) and non-LOS (NLOS) scenarios were measured, and a metal board was placed between Tx and Rx for the NLOS scenario. Note that there is no actual antenna array and no correlation effects among the antenna-array sets.

Since the Rayleigh distance [26] of the whole UCA is beyond 200 meters (at 30 GHz), in the data analysis, 16 consecutive virtual antennas are chosen as the virtual linear subarray within each sliding window along half of the virtual UCA as in Fig. 5. The size of virtual linear subarray is approximately 0.07 m. The Rayleigh distance of it is considered

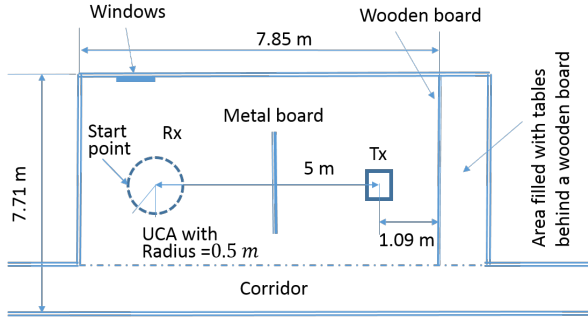


Fig. 4. Floorplan of the channel measurements in the basements [49].

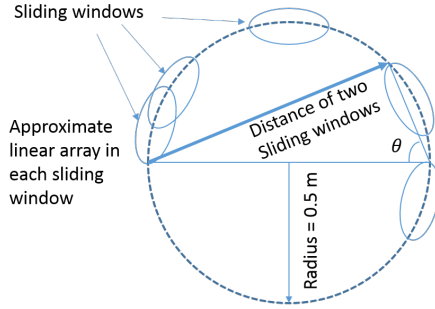


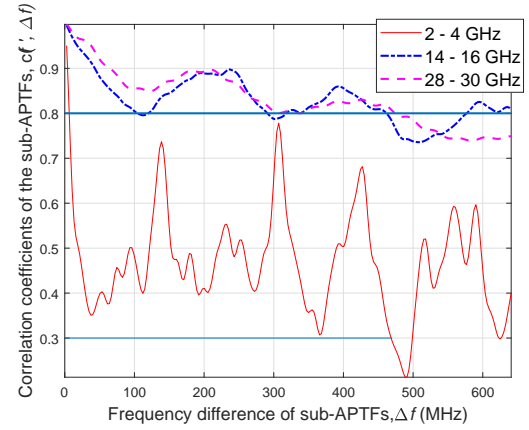
Fig. 5. Approximation of linear antenna subarrays [49].

shorter than the distance between Tx and Rx. To avoid the duplication in the content, more details of data processing can be found in Section III-C and Section IV.

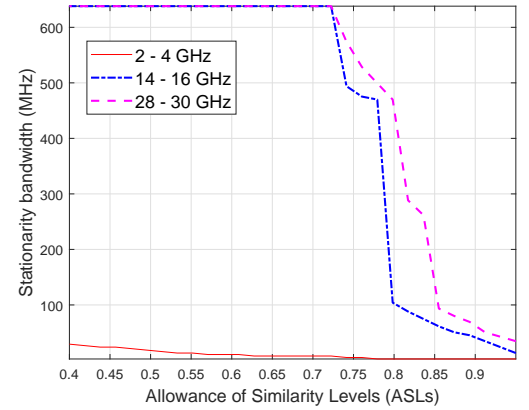
B. FSR Analysis

The calculation of frequency correlation coefficients was based on general APDP method applied in the frequency domain: averaging on antenna array as in Section II-C2. In order to reduce fluctuation in the results, the bandwidths of sub-APTFs in the sliding windows were 5% of the center frequency in each of the frequency bands. The results were consistent with those calculated when using a narrower bandwidth. The 5% bandwidth is assumed smaller than the FSRs of channels in all three bands.

In Fig. 6a, given that $ASL = 0.8$ as an example, it is clear that the stationary bandwidths at 14–16 GHz and 28–30 GHz bands are larger than those in 2–4 GHz band. In Fig. 6b, we illustrate the stationary bandwidths of all three bands for the ASLs from 0.4 to 0.95. It shows that the FSRs in 14–16 GHz and 28–30 GHz bands are much larger than that in 2–4 GHz band. The results shown are based on the averaging of first virtual linear subarray of the virtual UCA (16 virtual antennas out of 720). The FSRs based on other virtual linear subarrays around the whole UCA are also calculated, and the comparable estimation results between the 14–16 GHz band and 28–30 GHz band are found. However, all the estimated FSRs in mmWave frequency bands are much larger than those in sub-6 GHz frequency band for different ASLs. It is expected since the sizes of scatterers in the basement, such as the wall, ceiling, and windows, etc, are closer to the wavelength of the frequencies in 2–4 GHz bands than those in mmWave



(a)



(b)

Fig. 6. The FSRs of the channels, NLOS scenario: (a) correlation coefficients of the sub-APTFs and (b) stationary bandwidth vs. ASLs.

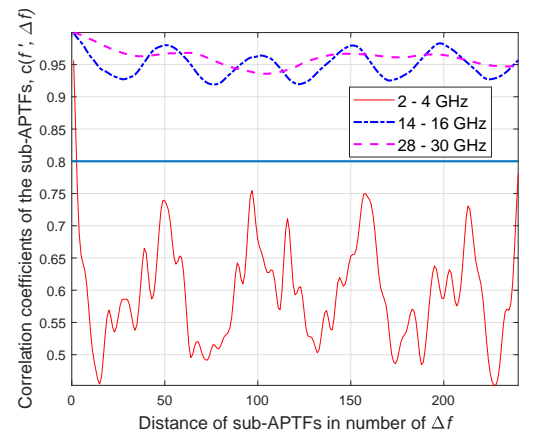


Fig. 7. Correlation coefficients of the sub-APTFs in the LOS scenario.

frequency bands. Those sounding signals are more interactive with those objects, which cause the statistical parameters change dramatically.

WINNER II channel models support 100 MHz system bandwidth, which is considered within one FSR. The FSR found in the 2–4 GHz band for the $ASL = 0.5$ is 18.69 MHz, which is much smaller, see Table I. One reason could be that the ASL chosen is too high. Another reason could be that the

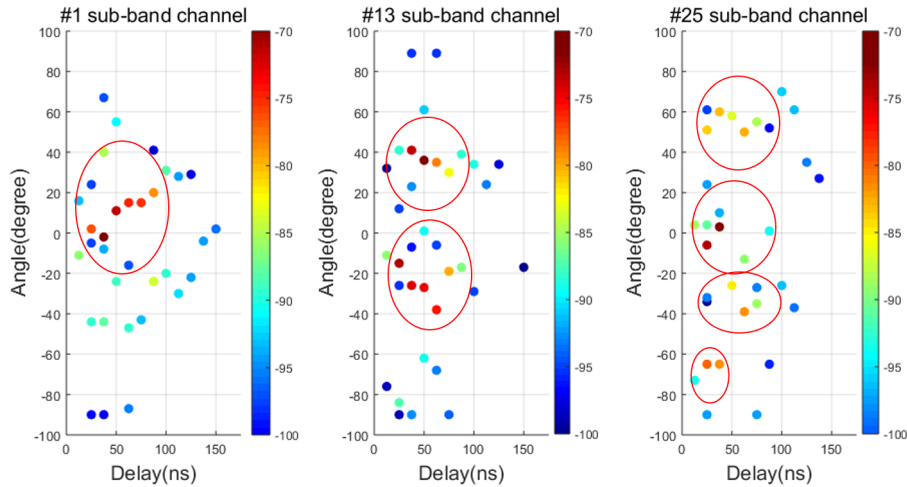


Fig. 8. Estimated MPCs in some of the sub-band channels from 2 to 4 GHz (LOS scenario).

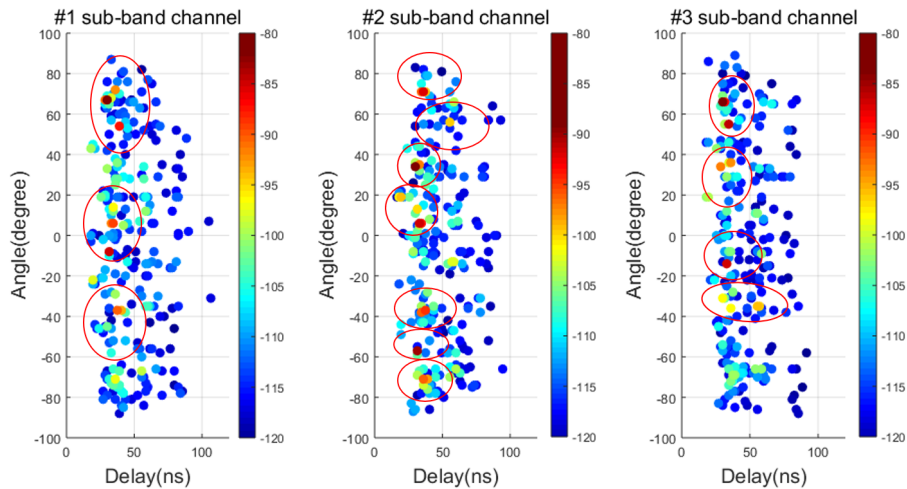


Fig. 9. Estimated MPCs in the sub-band channels from 28 to 30 GHz (LOS scenario).

TABLE I
SIZE OF FSRs IN A NLOS SCENARIO.

Frequency bands (GHz)	Size of FSRs in MHz for ASL = 0.5	Size of FSRs in MHz for ASL = 0.8
2–4	18.69	2.67
14–16	638.13	104.13
28–30	638.13	285.29

size of scatterers in the basement is closer to the wavelength of the frequencies in 2–4 GHz bands. The sounding signals in those frequencies are more interactive with the objects in this scenario than those in the scenarios defined in WINNER II. We can also observe that the correlation coefficients of sub-APTFs in the 2–4 GHz band are all higher than 0.3 for the stationary bandwidth within 467.25 MHz in Fig. 6a, i.e., the FSR is 467.25 MHz based on ASL = 0.3. Though this bandwidth seems too large, but for this specific scenario, it could be a reasonable size of FSR for 2–4 GHz band.

For the LOS scenario, the correlation coefficients of 14–16 GHz and 28–30 GHz frequency bands are very similar at

very high values as in Fig. 7. It is difficult to find an ASL to determine which frequency band has larger stationary bandwidth. The reason could be that the attenuation per meter of signals increases dramatically as the frequency goes higher. Therefore, the LOS component becomes more dominant in the measured CIRs at higher frequencies. The ratios of LOS component over NLOS components, i.e., K-factors [11], [12], are estimated based on the APDPs obtained from the first virtual linear subarray (similar results from other virtual linear subarrays). The K-factor in 2–4 GHz band is about 3 dB, it is about 12 dB in 14–16 GHz band and about 15 dB in 28–30 GHz band. It makes sense that the LOS component is more dominant in the measured CIRs in the 14–16 GHz and 28–30 GHz bands and the correlation coefficients estimated from those two bands mainly reflect the LOS component itself.

We notice that the FSRs (stationary bandwidths) are not linearly proportional to the center frequency in each measured frequency band. We can see that in both Fig. 6a and Fig. 7, the correlation coefficients of sub-APTFs are very close together for the 14–16 GHz and 28–30 GHz bands. Since the FSRs are

determined from the correlation coefficients of sub-APTFs by given ASLs, the FSRs are comparable in the 14-16 GHz band and in the 28-30 GHz band based on the results shown in Fig. 6b and Table I, especially when the given ASL is smaller than approximately 0.72. The sizes of FSRs in different frequencies are not similar to that of defining the coherence bandwidth (fractional bandwidth), 10% of the center frequency (rule of thumb), within which the channel is approximately considered frequency flat [57].

C. Variation of Statistical Properties

Since the estimated FSRs are smaller than 2 GHz for the channels in those three frequency bands, the WSS assumption is only valid within one FSR, not the whole bandwidth of 2 GHz. Therefore, those channels should be considered as FnS. For the convenience, we equally split the bandwidth of 2-4 GHz band into 25 sub-bands, each with 80.1 MHz bandwidth (30 frequency points $\times \Delta f$, $\Delta f = 2.67$ MHz). We also equally split the bandwidth of 28-30 GHz band into 3 sub-bands, each with 667.5 MHz bandwidth (250 frequency points). The (stationary) bandwidths of the sub-band channels chosen are close to those of the standard channel models, such as WINNER II (100 MHz in sub-6 GHz bands) and METIS (500 MHz or larger in mmWave bands).

We choose 30 dB and 40 dB dynamic range of the sub-band CIRs in 2-4 GHz and in 14-16/28-30 GHz frequency bands, respectively. SAGE [58], [59] is used in the estimation of azimuth angle of arrival (AoA), time of arrival (ToA), and amplitude of multi-path components (MPCs) in each sub-band channels based on the first 16-virtual linear subarray. We estimate 35 MPCs from the sub-band channels within 2-4 GHz band, and 250 MPCs from those within 28-30 GHz band (the number of estimated MPCs are comparable to those in [44], [60]). The results are illustrated in Fig. 8 and Fig. 9. We can observe clearly different delays and angles of the MPCs with higher powers in Fig. 8, and slight differences of those in Fig. 9. The MPCs of sub-band channels based on other 16 virtual linear subarrays are also estimated. Similar phenomenon was found. We do not show them here for conciseness purposes.

1) *Statistical Properties in the Frequency Domain:* The autocorrelation function is normally used to present the statistical property of wireless channel in the time domain [11], [61]. In the frequency domain, the frequency correlation function (FCF) can be used to represent the statistical properties of channels. Similarly, the FCF can be defined as

$$R_H(f_1; f_2) = E\{H^*(f_1)H(f_2)\} \quad (8)$$

where $H(f)$ is transfer function (Fourier transformation of CIR), and $[\cdot]^*$ and $E\{\cdot\}$ are conjugate operator and expectation operator, respectively.

2) *Variation of FCFs of Sub-Band Channels:* The FCFs of sub-band channels are shown in Fig. 10. The FCFs of selected sub-band channels within the 2-4 GHz band are apparently different in Fig. 10a (only showing the most different ones) and the maximum difference is 0.2. The FCFs of sub-band channels within the 28-30 GHz band are slightly different

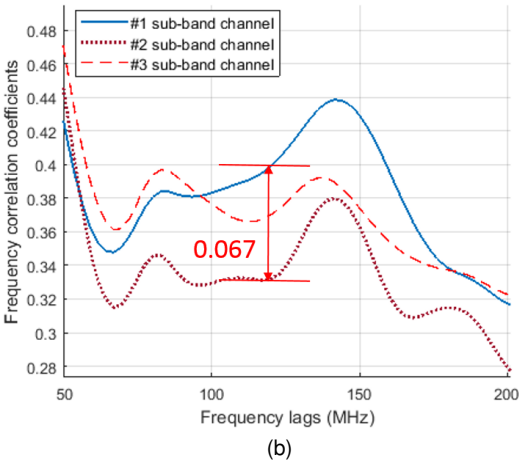
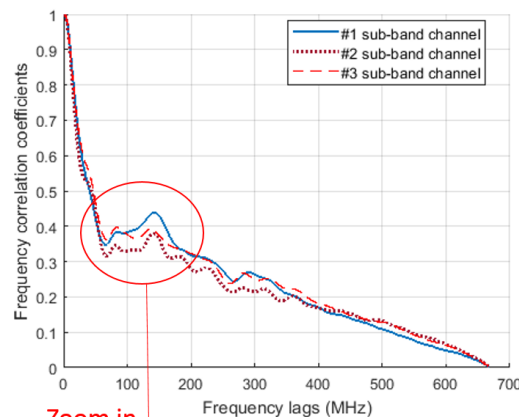
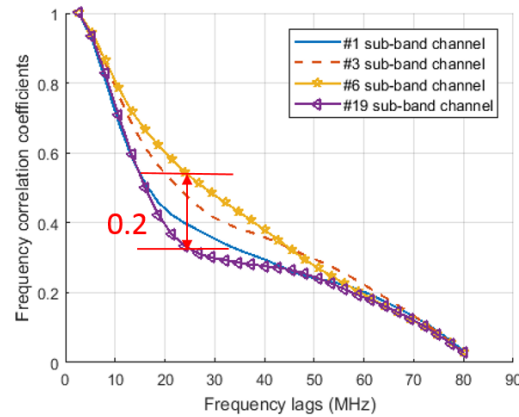


Fig. 10. The FCFs of the sub-band channels, NLOS scenario: (a) within 2-4 GHz band and (b) within 28-30 GHz band.

to each other and the maximum difference is 0.067. This is consistent with the MPC estimations in Fig. 8 and Fig. 9. Note that the results here can be an explanation about the higher values of correlation coefficients in mmWave frequency bands in Fig. 6a.

IV. A FNS CHANNEL MODEL

To the best of our knowledge, the current standard channel models are not suitable to model the measured FnS channels described previously. Though the UWB channel models [35],

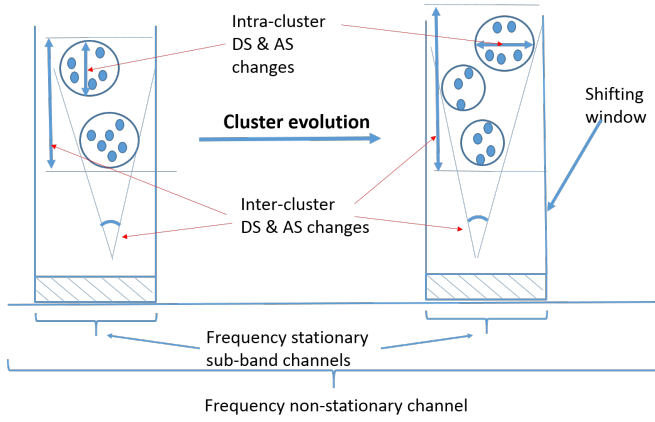


Fig. 11. Cluster evolution in the frequency domain.

[62] are FnS channel models, but they do not address the 14–16 GHz and 28–30 GHz frequency bands. In addition, they are very different from the standard channel models. Therefore, we propose a general FnS channel model for B5G wireless communication channels. The principle of proposed FnS channel model is designed based on the studies of frequency stationary regions and the combination of sub-band channels (need to use the real measured THz channel parameters in the model for modeling the THz FnS channels). There is no frequency limitation. However, the current modeling of sub-band channels is based on the 3GPP channel model. This limits the overall FnS model to 100 GHz, which is the same as that for 3GPP channel models. Due to limited measurement data, we focus on modeling the channels in sub-6 GHz and mmWave frequency bands.

A. FnS Channel Modeling

Given a static FnS wireless channel where the bandwidth covers a few FSRs, we assume that there is a shifting window in the frequency domain with the bandwidth covering only one FSR, and it moves over each FS sub-band channel within such FnS channel. If the sub-band channels are non-overlapping to each other, then the whole FnS channel is the sum of all sub-band channels. It can be written as

$$\mathbf{h}(\tau) = \sum_{o=1}^O \mathcal{F}^{-1}[\delta(f - f_{co})]h^{\text{sub}}(\tau, f_{co}) \quad (9)$$

where there are O sub-band channels, $o = 1, 2, \dots, O$, f_{co} denoting the center frequency $f_{c1}, f_{c2}, \dots, f_{cO}$ of sub-band channel, and $\mathcal{F}^{-1}[\cdot]$ is the inverse Fourier transformation.

For each sub-band channel, i.e., a wideband channel [11], can be modeled as

$$\begin{aligned} h^{\text{sub}}(\tau, f_{co}) = & \sum_{u=1}^U \sum_{v=1}^V a_{u,v}(f_{co}) \exp(j\beta_{u,v}) \\ & \times \delta(\tau - \tau_u(f_{co}) - \tau_{u,v}(f_{co})) \\ & \times \delta(\theta - \theta_u(f_{co}) - \theta_{u,v}(f_{co})) \end{aligned} \quad (10)$$

where we assume there are U clusters and V rays in each cluster, $u = 1, 2, \dots, U$, $v = 1, 2, \dots, V$. The amplitude of a

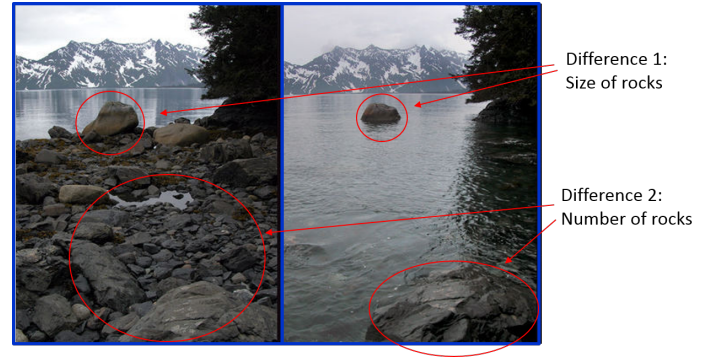


Fig. 12. Tidal variation, as a metaphor to explain the cluster evolution in the frequency domain.

ray is denoted as $a_{u,v}(f_{co})$ and $a_u(f_{co})^2 = \sum_{v=1}^V a_{u,v}(f_{co})^2$ represents the cluster power. The inter-cluster delay and angle are denoted as $\tau_u(f_{co})$ and $\theta_u(f_{co})$. Due to scattering, reflection, etc. as the rays travel through the channel, $\exp(j\beta_{u,v})$ represents the random phases of rays and $\beta_{u,v}$ is uniformly distributed, $\beta_{u,v} \sim \text{Uni}[-\pi, \pi]$.

Note that the model proposed are only related to small-scale parameters. We do not address large-scale parameters, such as path loss, shadowing, etc.

B. Cluster Evolution in the Frequency Domain

Though the multi-band OFDM technologies can be used to measure the channels with very broad bandwidth [63], we cannot model each of “narrower” OFDM channels and simply combine them as one channel. The frequency-dependent statistical parameters of those multi-band channels need to be studied and the frequency consistency among multi-band channels needs to be considered in the model. Therefore, a novel frequency domain cluster evolution is proposed for the implementation of the FnS model as shown in Fig. 11. It describes the relationship among those sub-band channels, and maintains each two consecutive sub-band channels at a reasonable similarity level. This also assures the frequency consistency of sub-band channels, i.e., the similarity level of simulated sub-band channels is as close as possible to that of the sub-band channels found in the measurement data analysis.

There are two features of cluster evolution in the frequency domain based on the measured time-invariant channels in Section III-A. First, it describes the variations of channel characteristics within the bandwidths of those channels. Second, the inter-cluster parameters are not constant numbers (for one channel scenario), they are described by trends due to the variations of channel characteristics within the frequency range of a FnS channel. Tidal variation can be used as a metaphor to describe the cluster evolution in the frequency domain as Fig. 12. We assume that the high tide and low tide situations represent two estimated cluster-maps of two sub-band channels. There are two categories of differences we can observe from the high tide and low tide situations: the number of rocks and the size of rocks. Those are used to describe the cluster differences in two consecutive sub-band channels in the frequency domain cluster evolution.

TABLE II
PARAMETERS OF SUB-BAND CHANNELS (NLOS SCENARIO, 2–4 GHz).

Parameters	Mean	Maximum
(Inter-cluster) DSs, $\sigma_\tau(f_{co})$ (ns)	15.5	22.3
Standard deviation of ray delays (ns)	46	74.8
Standard deviation of inter-cluster angles, $\sigma_\theta(f_{co})$ ($^\circ$)	49.6	63.6
Standard deviation of intra-cluster ray angles ($^\circ$)	6.7	9.6

TABLE III
PARAMETERS OF SUB-BAND CHANNELS (NLOS SCENARIO, 28–30 GHz).

Parameters	Mean	Maximum
(Inter-cluster) DSs, $\sigma_\tau(f_{co})$ (ns)	7.9	9.4
Standard deviation of ray delays (ns)	12.6	14.8
Standard deviation of inter-cluster angles, $\sigma_\theta(f_{co})$ ($^\circ$)	49.7	51.2
Standard deviation of intra-cluster ray angles ($^\circ$)	8.3	8.8

The idea is based on that a cluster is a bunch of estimated MPCs, which represent the interaction between the transmitting signals and a bunch of correlated scatterers (objects). They are defined and modeled with reasonable discrepancies based on the frequency and bandwidth of channel. The proposed algorithm of cluster evolution in the frequency domain is similar to the birth-death processes used in [30]–[32]. However, we simply use cluster survival rate instead of the cluster birth rate and death rate as follows:

- Track the survival probability of each single cluster by

$$P_{\text{survival}} = \exp(-\lambda O') \quad (11)$$

when it evolves from one sub-band channel into another one. The rate parameter is denoted by λ , and O' is the number of sub-band channels one cluster survives.

- Pre-define the number of clusters for all sub-band channels by trend. When the clusters evolve to another sub-band channel, only generate new clusters to substitute the dead or if the number of clusters increases.
- In a new sub-band channel, use the updated inter-cluster parameters by the trends when generating new cluster. Update all the intra-cluster parameters of the clusters by the trends.

Note that it is primary to consider the cluster evolution in the frequency domain for a static channel. For the time-variant channels, which consists of a few or many snapshots, the cluster evolution in the frequency domain can be processed snapshot by snapshot since each snapshot is considered as a static channel.

C. Statistical Parameters of Measured Sub-Band Channels

1) *Parameters Estimation*: As described in Section III-C to split the 2 GHz band into sub-band channels, we estimated the MPCs of each sub-band. For each FnS CIR, it consist of delay/frequency 750 points. We split the 2–4 GHz band

(750 frequency points) into 25 sub-band channels (each having 30 frequency points) and split the 28–30 GHz band (750 frequency points) into 3 sub-band channels (each having 250 frequency points). The numbers of clusters estimated by K-mean [64] are different in different sub-band channels due to the FnS property within 2 GHz bandwidth. We then apply visual judgement on the estimated clusters in each sub-band channel. We determine 7 clusters for each sub-band channel within the 2–4 GHz band and 10 clusters for each sub-band channel within the 28–30 GHz band, which are the highest reasonably estimated cluster numbers from those 30 sub-band channels within 2–4 GHz band and 3 sub-band channels within 28–30 GHz band. It enables us to capture the cluster properties of all the sub-band channels in different frequencies. The procedure for the parameter estimations of all the sub-band channels can be described by the pseudo code as below:

- Determine the stationary bandwidth of sub-band channels, and equally split the FnS channel into FS sub-band channels according to the FSR;
- while** ($o < \text{number of sub-band channels}$) **do**
- Estimate the delay, angle and the amplitude of the MPCs in current sub-band channel by SAGE;
- Cluster the MPCs;
- Estimate the inter-cluster and intra-cluster parameters;
- end while**
- Find out the statistics of the inter-cluster and intra-cluster parameters of all sub-band channels.

The statistics of inter-cluster and intra-cluster parameters of all the sub-band channels are illustrated in Table II and Table III. Due to that it is similar to estimate the parameters from the 14-16 GHz measurement data and for the compact of content, we do not show the results.

Note that the parameters in the tables were estimated based on one channel measurement campaign. They are unique and considered as a deterministic description of the radio environmental [11] (as well as survival probability [31]). We do not recommend to use those parameters in the prediction of the characteristics of channels in other environments. Much more work is required to determine the channel parameters used in this purpose and we leave it in the future at the moment. In addition, there are specially developed ToA/AoA algorithms that are used in the parameter estimation of UWB channels [34], [65], [66]. We expect that some of the algorithms could be used in the parameter estimations of FnS mmWave channels. However, further studies are required to verify the feasibility of them and we leave it in the future.

2) *Trends of Statistical Parameters*: The trends of statistical parameters through all the sub-band channels need to be estimated and those are the key factors in the implementation of the FnS model. In [36], the trends of (inter-cluster) AS and DS among sub-band channels, within 6 GHz bandwidth, were described as exponential functions (similar trends are used in the 5GCM and latest 3GPP channel models in the study of the frequency dependent parameters from 1 GHz to 100 GHz). However, due to limited number of sub-band channels

available for data analysis in our cases, we can only observe the variation of those statistical parameters among sub-band channels. We do not show them due to the page limit of paper. Since it is not sufficient to find the exact trends of them, we use linear trends instead, from the mean to the maximum.

V. GENERATION OF FNS CHANNEL COEFFICIENT

A. Generation of One Sub-Band Channel Coefficient

In this section, a revised 3GPP simulation model is used to describe each of the sub-band channels, and this model is suitable in the implementation of cluster evolution in the frequency domain.

Step 1: Generate random delays based on exponential distribution as

$$\tau'_u(f_{co}) = -r_\tau(f_{co})\sigma_\tau(f_{co})\ln(X_u) \quad (12)$$

where $r_\tau(f_{co})$ is the delay distribution proportionality factor, $\sigma_\tau(f_{co})$ is the DS (inter-cluster DS in this paper as well), $\ln(\cdot)$ is natural logarithm, and X_u is the random number following uniform distribution, $X_u \sim \text{Uni}(0, 1)$. Normalize delays $\tau'_u(f_{co})$ by subtracting the minimum delay and aligning them in descending order. Then we get the inter-cluster delays $\tau_u(f_{co})$ as

$$\tau_u(f_{co}) = \text{sort}(\tau'_u(f_{co}) - \min(\tau'_u(f_{co}))). \quad (13)$$

Step 2: The inter-cluster powers are generated as

$$P'_u(f_{co}) = \exp(-\tau_u(f_{co}) \frac{r_\tau(f_{co}) - 1}{r_\tau(f_{co})\sigma_\tau(f_{co})}) \quad (14)$$

$$P_u(f_{co}) = \frac{P'_u(f_{co})}{\sum_{u=1}^U P'_u(f_{co})} \quad (15)$$

where $P'_u(f_{co})$ is the random power following an exponential delay distribution, $P_u(f_{co})$ is the normalized inter-cluster power. Note that there is no shadowing in the model, since we focus on the small-scale parameters.

Step 3: Inter-cluster angles are generated as

$$\theta_u(f_{co}) = \theta_u^{\text{mean}}(f_{co}) + \sigma_\theta(f_{co})Z_u \quad (16)$$

where the mean angle of cluster and standard deviation of inter-cluster angles are denoted by $\theta_u^{\text{mean}}(f_{co})$ and $\sigma_\theta(f_{co})$. The random number Z_u follows standard normal distribution, $Z_u \sim \text{N}(0, 1)$.

Step 4: In order to make the cluster evolution possible in the frequency domain, we modify the description of rays in the 3GPP model. We introduce certain variables in the modeling of rays and we let the ray powers also follow exponential distributions as cluster powers. In the generations of intra-cluster parameters, such as delay of ray $\tau_{u,v}(f_{co})$, amplitude of ray $a_{u,v}(f_{co})$, and angle of ray $\theta_{u,v}(f_{co})$, we simply use intra-cluster parameters to substitute the corresponding inter-cluster parameters in (12)–(16), except that we use standard deviation of ray delays to substitute $\sigma_\tau(f_{co})$ in (12). The sum of rays powers within one cluster should be equal to the power of such cluster, i.e., $P_u(f_{co}) = \sum_{v=1}^V P_{u,v}(f_{co})$, $P_{u,v}(f_{co})$ is the ray power.

Step 5: Scale the intra-cluster parameters based on inter-cluster parameters and sum up the ray powers (complex

numbers) as the cluster powers. Finally, the sub-band channel coefficient can be generated as described in (10).

In the LOS case: Similar to 3GPP and ITU-R models, the sub-band channel coefficient in LOS case is the combination of a single LOS ray and a scale-down NLOS channel coefficient, generated as above. Note that this generation method explains the data analysis results in Fig. 7.

B. Cluster Evolution

In the implementation of FnS channel model, we only generated the channel coefficient of first sub-band channel as described above. After that, we apply the frequency domain cluster evolution in the generation of the rest of sub-band channel coefficients according to the description in Section IV-C2. For general purpose of the model, we suggest using trends to describe 5 frequency-dependent parameters in the frequency domain cluster evolution procedure. Those 5 parameters are (inter-cluster) DSs, standard deviation of inter-cluster angles, standard deviation of ray delays, standard deviation of intra-cluster ray angles, and number of clusters in each sub-band channel.

Based on the limited data, we choose to describe 4 parameters by linear trends from the mean value to the maximum value as in Table II and Table III. We do not use the linear trend for the number of clusters in the sub-band channels since we do not have enough data to prove the trend. We fix the cluster number for all sub-band channels instead.

C. Adding Up Sub-Band Channels

Once all the sub-band channel coefficients are generated, we add them up as one FnS channel coefficient. The idea is similar to the working principle of VNA in appendix IV.A.4 of [62]. The relationship of frequency/delay intervals and frequency/delay points, that are used to describe the sub-band channels in the time and frequency domains, can be simply regulated as those in fast Fourier transformation (FFT) [67]. However, the adding-up step is a straightforward combination of sub-band channels either in the frequency domain or in the time domain. Note that there is no Fourier transformation involved.

Fig. 13 is an example of adding up two sub-band channels. Similarly, we can add up more sub-band channels in the same manner. On the right hand side of the figure, the bandwidth of FnS sounding signal $\mathbf{H}(f)$ is f_s Hz, and it consists of Q frequency points with equal frequency interval of f_i Hz. We split $\mathbf{H}(f)$ into two sub-band sounding signals $H^{\text{sub}}(f, f_{c1})$ and $H^{\text{sub}}(f, f_{c2})$ with equal bandwidths of $Q/2$ frequency points while keeping the frequency interval as f_i Hz. Then, we Fourier transform those sub-band sounding signals into the time domain, and transmit them through the same static environment. On the left hand side of the figure, each delay bin of sub-band CIRs $h^{\text{sub}}(\tau, f_{c1})$ and $h^{\text{sub}}(\tau, f_{c2})$ is $2t_s$ ns ($t_s = 1/f_s$), and the lengths of $h^{\text{sub}}(\tau, f_{c1})$ and $h^{\text{sub}}(\tau, f_{c2})$ are both τ ns ($\tau = 1/f_i$). After adding them up, each delay bin of FnS-CIRs $\mathbf{h}(\tau)$ is t_s ns, and the length of $\mathbf{h}(\tau)$ is still τ ns.

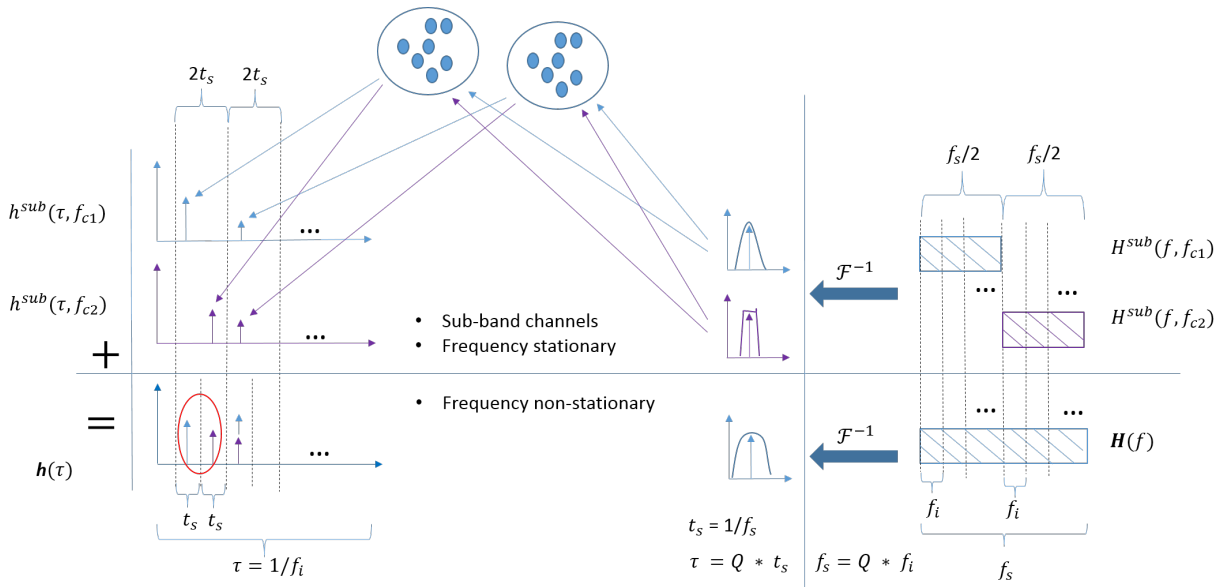


Fig. 13. Example of adding up two sub-band channels as one FnS channel.

Fig. 13 also shows the main difference between the FS and FnS channels in the channel modeling. The power in each delay bin of FS-CIR ($h^{sub}(\tau, f_{c1})$ and $h^{sub}(\tau, f_{c2})$) relate to only one cluster and those powers are uncorrelated. This is the WSS assumption in the frequency domain [11], [12]. While the powers in the second and third delay bins of FnS-CIR ($h(\tau)$) relate to the same cluster. The powers of those two delay bins are correlated and this violates WSS assumption in the frequency domain.

D. Implementation Details

The procedure of generating a FnS channel coefficient can be described as the pseudo code below:

- 1: Determine the number of sub-band channels, the number of clusters in each sub-band channel, and the number of rays within each cluster;
- 2: Determine the trends of (inter-cluster) DS and AS, and the intra-cluster DS and AS for all the sub-band channels;
- 3: **if** (first sub-band channel) **then**
- 4: Generate the first sub-band channel coefficient according to Section V-A, and save the delay, angle and power of each cluster;
- 5: **else**
- 6: **while** ($o < \text{number of sub-band channels}$) **do**
- 7: Track and calculate the cluster survival probability by (11) for each single cluster when it evolves to current sub-band channel;
- 8: Once one cluster dies or the cluster number increases, generate a new cluster with the (inter-cluster) ASs and DSs following the trends. If the cluster survives, keep the cluster delay, angle, and power in the current sub-band channel;
- 9: Update all intra-cluster ASs and DSs by trends;
- 10: Regenerate intra-cluster delays, powers, and angles of each cluster;

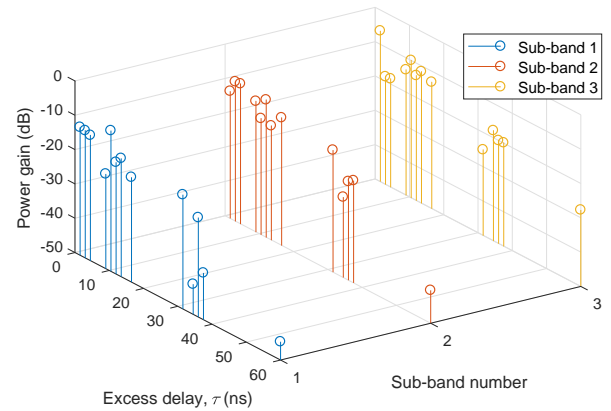


Fig. 14. Frequency consistent simulated sub-band CIRs, 28–30 GHz band.

- 11: Generate the current sub-band channel coefficient;
- 12: **end while**
- 13: **end if**
- 14: Adding up all the sub-band channel coefficients as in Section V-C.

VI. VALIDATION OF THE FNS CHANNEL MODEL

A. Simulation of FnS Channels

In simulations, the parameters used in the generation of the first sub-band channel coefficients are the mean values in Table II and Table III. In the procedure of cluster evolution in the frequency domain, the linear trends of those parameters are used, from the mean values to the max values. However, we do not use trends of the numbers of clusters against sub-band channels in our cases. We fixed the number of clusters to 20 and number of rays within each cluster to 20 for all sub-band channels. Fig. 14 shows the sub-band CIRs from one simulation. The cross-correlation coefficients among the

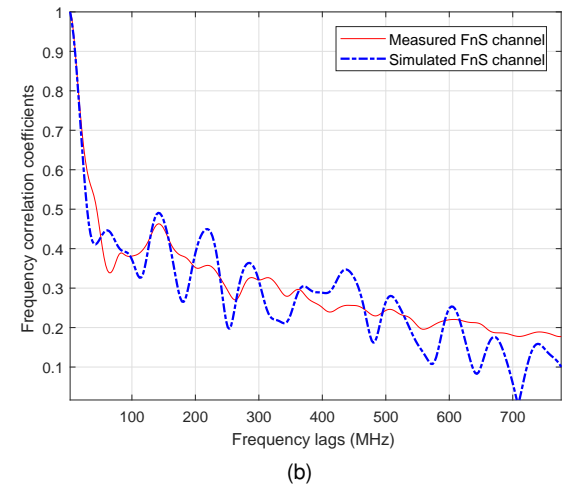
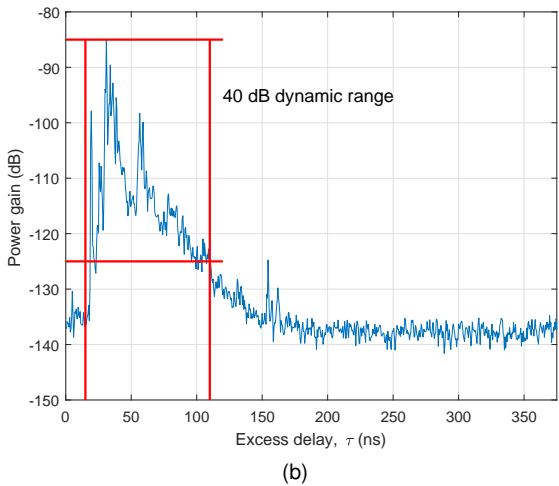
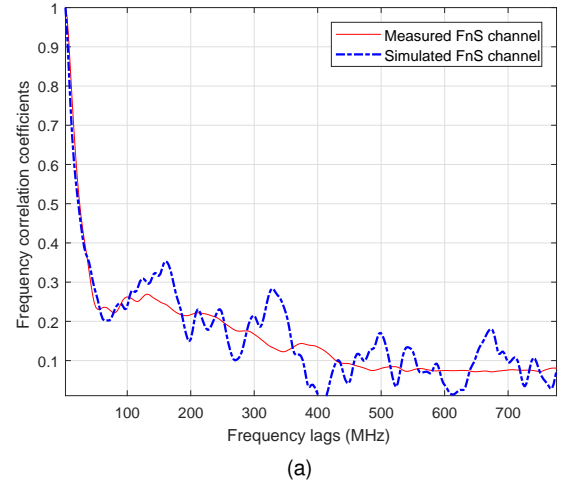
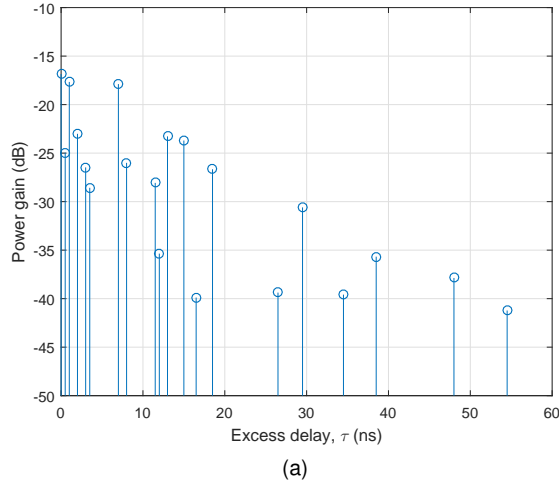


Fig. 15. FnS channels, NLOS scenario, 28–30 GHz band: (a) simulated FnS-CIR and (b) measured FnS-CIR.

Fig. 16. FCF approximations, NLOS scenario: (a) 2–4 GHz band and (b) 28–30 GHz band.

sub-band CIRs are between 0.785 and 0.8545. In Fig. 15a, one simulated FnS-CIR for the channel in 28–30 GHz band is shown. It represents the measured FnS-CIR within 40 dB dynamic range in Fig. 15b. In Fig. 15a, the absolute gain levels of the simulated CIR, in the range of $[-50 -10]$ dB, are normalized values. It can be scaled by large-scale parameters, then, it can be close to the gain levels of measured CIR, in the range of $[-150 -80]$ dB, in Fig. 15b. However, we only focus on the small-scale parameter and we keep the gain levels of simulated CIR as normalized values.

The measured FnS channels were used as the references in the validation of FnS channel model. We used the FCF of the simulated FnS channel to approximate the FCF of the measured FnS channel by optimization based on least mean-square (LMS) method. During the frequency domain cluster evolution process, we only changed the cluster survival probability and the initial values of the random numbers, X_u and Z_u in (12) and (16). We notice that for a good approximation, λ values in cluster survival probability (11) found by optimization algorithm were between 0.05 and 0.1 in the sub-band channels within the 2–4 GHz band, and between

0.025 and 0.05 in those within the 28–30 GHz band. We also found that the clusters can survive 1–15 sub-band channels (25 in total) within the 2–4 GHz band in the cluster evolution. Since there are only 3 sub-band channels within the 28–30 GHz band, finding that the clusters survived for all 13 sub-band channels was expected. The results of approximations can be found in Fig. 16. We can see that the simulations could follow the measured data in both the 2–4 GHz and 28–30 GHz bands very well. The difference of those two bands between the simulation and measurement within first 150 MHz frequency lags is about 3% in the LMS optimization. Due to using a similar procedure for the verification of the model for 14–16 GHz band and the similar results, we do not show the details for conciseness purposes.

Note that if we fix the number of clusters to 10 in each sub-band channels (same as that used in the parameters estimation in Section IV-C), the FCF approximation results are similar. However, the FCFs of simulated FnS channel are generally fluctuating with larger deviation surrounding the FCFs of measured FnS channels.

B. Amplitude Distribution of Simulated FnS channels

In the literature, the UWB channel models address the FnS channels [62]. The Nakagami- m distribution [68], [69] was used to describe the signal amplitudes of UWB channels and the estimated m -values were close to 1. Since the proposed FnS channel model can be used to model UWB channels, we expect that the signal amplitudes of simulated FnS channels also follow Nakagami- m distributions. However, we do not use m values to affect the performance of the proposed FnS model, because the related mathematical deductions for the fading properties of FnS channels are difficult and challenging. It is due to that the different durations of delay bins between those in sub-band channels and those in FnS channels as shown in Fig. 13. We have been unable to find the related mathematical explanation in the literature. Instead, the m values are estimated based on massive generated FnS CIRs, which is similar to estimating the statistical parameters based on the real channel measurement data.

We simulate the FnS channel model 50,000 times working in the 28–30 GHz band for the NLOS case. In order to increase the chance that the cluster powers of sub-band FS-CIRs can fall into the same delay bin of the FnS-CIR when adding up the sub-band channels, we increase the number of clusters in the sub-band channels to 60 (20 clusters was used formerly).

We use Nakagami- m distribution to approximate the amplitude in each delay bin of simulated FnS-CIRs. For most of the delay bins, the estimated m -values are around 0.83 and 1.44. If increase the number of clusters in each sub-band channel from 60 to higher values, the m -values increase correspondingly. Similar results are found in the simulations of FnS-CIRs in 2–4 GHz band for NLOS case. However, in order to let the m -values close to 1, the number of clusters in each sub-band channel used in the simulation is about 100.

VII. CONCLUSIONS

A general APDP method has been introduced to determine the stationarity regions of wireless channels in the time, frequency, and spatial domains. It is an extension of the original APDP method used to study the stationarities of channels in time and spatial domains. We have applied this method to an empty basement channel measurements in a sub-6 GHz frequency band (2–4 GHz) and two mmWave frequency bands (14–16 GHz and 28–30 GHz). We have found that the FSRs of channels in the mmWave frequency bands are larger than those in the sub-6 GHz frequency band. We have also addressed the FnS properties of channels in all the three measured frequency bands.

To the best of our knowledge, the existing 5G standard channel models did not consider frequency non-stationarity and are not suitable for modeling the measured FnS channels in our case. Therefore, we have proposed a novel B5G FnS channel model that is suitable to model wireless channels in all frequency bands. We have proposed to split a FnS channel into a few FS sub-band channels and model them one by one. Finally, these FS sub-band channel models are combined as one FnS channel model by taking into account the frequency-domain cluster evolution and frequency consistency of sub-band channels. The FCFs of the simulated and measured FnS

channels have been compared, showing that the simulations can successfully approximate the measurement data in both the 2–4 GHz and 28–30 GHz frequency bands. This has partly verified the validity of the proposed FnS channel model.

REFERENCES

- [1] C.-X. Wang, F. Haider, and X. Gao, et al., "Cellular architecture and key technologies for 5G wireless communication networks," *IEEE Commun. Mag.*, vol. 52, no. 2, pp. 122–130, Feb. 2014.
- [2] C.-X. Wang, J. Bian, J. Sun, W. Zhang, and M. Zhang, "A survey of 5G channel measurements and models," *IEEE Commun. Surveys Tuts.*, vol. 20, no. 4, pp. 3142–3168, 4th Quart., 2018.
- [3] A. F. Molisch and F. Tufvesson, "Propagation channel models for next-generation wireless communications systems," *IEICE Trans. Commun.*, vol. E97-B, no. 10, pp. 2022–2034, Oct. 2014.
- [4] W. Roh, J. Y. Seol, and J. Park, et al., "Millimeter-wave beamforming as an enabling technology for 5G cellular communications: theoretical feasibility and prototype results," *IEEE Commun. Mag.*, vol. 52, no. 2, pp. 106–113, Feb. 2014.
- [5] M. K. Samimi and T. S. Rappaport, "3-D millimeter-wave statistical channel model for 5G wireless system design," *IEEE Trans. Microw. Theory Techn.*, vol. 64, no. 7, pp. 2207–2225, July 2016.
- [6] K. Guan, G. Li, and T. Kürner, et al., "On millimeter wave and THz mobile radio channel for smart rail mobility," *IEEE Trans. Veh. Technol.*, vol. 66, no. 7, pp. 5658–5674, Jul. 2017.
- [7] X. Wu, C.-X. Wang, J. Sun, J. Huang, R. Feng, Y. Yang, and X. Ge, "60-GHz millimeter-wave channel measurements and modeling for indoor office environments," *IEEE Trans. Antennas Propag.*, vol. 65, no. 4, pp. 1912–1924, Apr. 2017.
- [8] S. Priebe and T. Kürner, "Stochastic modeling of THz indoor radio channels," *IEEE Trans. Wireless Commun.*, vol. 12, no. 9, pp. 4445–4455, Sept. 2013.
- [9] S. Kim and A. G. Zajić, "Statistical characterization of 300-GHz propagation on a desktop," *IEEE Trans. Veh. Technol.*, vol. 64, no. 8, pp. 3330–3338, Aug. 2015.
- [10] P. Bello, "Characterization of randomly time-variant linear channels," *IEEE Trans. Commun.*, vol. 11, no. 4, pp. 360–393, Dec. 1963.
- [11] A. F. Molisch, *Wireless Communications, Second Edition*. John Wiley & Sons, 2011.
- [12] A. Paulraj, R. Nabar, and D. Gore, *Introduction to Space-Time Wireless Communications*. Cambridge University Press, 2003.
- [13] K. Pekka, J. Meinilä, and L. Hentilä, et al., "WINNER II channel models," D1.1.2 V1.2, IST-4-027756, WINNER II Deliverable, 4, Feb. 2008.
- [14] P. Heino, J. Meinilä, and P. Kyösti, et al., "WINNER+ final channel models", ver 1.0, Jun. 2010. Available: <http://projects.celticinitiative.org/winner+/WINNER+ Deliverables/D5.3 v1.0.pdf>.
- [15] Report ITU-R M.2135-1 "Guidelines for evaluation of radio interface technologies for IMT-Advanced", Dec. 2009.
- [16] 3GPP T.R. 38.901, "Study on channel model for frequencies from 0.5 to 100 GHz", V15.0.0, June 2018.
- [17] S. Jaeckel, L. Raschkowski, K. Börner, and L. Thiele, "QuADRIa: A 3-D multi-cell channel model with time evolution for enabling virtual field trials," *IEEE Trans. Antennas Propag.*, vol. 62, no. 6, pp. 3242–3256, Jun. 2014.
- [18] R. Verdone and A. Zanella, *Pervasive Mobile and Ambient Wireless Communications: COST Action 2100*. Springer Science & Business Media, 2012.
- [19] Q. Zhu, H. Li, and Y. Fu, et al., "A novel 3D non-stationary wireless MIMO channel simulator and hardware emulator," *IEEE Trans. Commun.*, vol. 66, no. 9, pp. 3865–3878, Sept. 2018.
- [20] J. Bian, J. Sun, and C.-X. Wang, et al., "A WINNER+ based 3D non-stationary wideband MIMO channel model," *IEEE Trans. Wireless Commun.*, vol. 17, no. 3, pp. 1755–1767, Mar. 2018.
- [21] C.-X. Wang, A. Ghazal, B. Ai, P. Fan, and Y. Liu, "Channel measurements and models for high-speed train communication systems: a survey," *IEEE Commun. Surveys Tuts.*, vol. 18, no. 2, pp. 974–987, 2nd Quart., 2016.
- [22] Y. Yuan, C.-X. Wang, Y. He, M. M. Alwakeel, and H. Aggoune, "3D wideband non-stationary geometry-based stochastic models for non-isotropic MIMO vehicle-to-vehicle channels," *IEEE Trans. Wireless Commun.*, vol. 14, no. 12, pp. 6883–6895, Dec. 2015.
- [23] Y. Liu, C.-X. Wang, C. F. Lopez, and X. Ge, "3D non-stationary wideband circular tunnel channel models for high-speed train wireless communication systems," *Sci. China Inf. Sci.*, vol. 60, no. 8, Aug. 2017.

- [24] Y. Liu, C.-X. Wang, J. Huang, J. Sun, and W. Zhang, "Novel 3-D nonstationary mmWave massive MIMO channel models for 5G high-speed train wireless communications," *IEEE Trans. Veh. Technol.*, vol. 68, no. 3, pp. 2077–2086, Mar. 2019.
- [25] Y. Liu, A. Ghazal, C.-X. Wang, X. Ge, Y. Yang, and Y. Zhang, "Channel measurements and models for high-speed train wireless communication systems in tunnel scenarios: a survey," *Sci. China Inf. Sci.*, vol. 60, no. 8, doi: 10.1007/s11432-016-9014-3, Oct. 2017.
- [26] J. Huang, C.-X. Wang, R. Feng, J. Sun, W. Zhang, and Y. Yang, "Multi-frequency mmWave massive MIMO channel measurements and characterization for 5G wireless communication systems," *IEEE J. Sel. Areas Commun.*, vol. 35, no. 7, pp. 1591–1605, July 2017.
- [27] X. Gao, O. Edfors, F. Tufvesson, and E. G. Larsson, "Massive MIMO in real propagation environments: do all antennas contribute equally?" *IEEE Trans. Commun.*, vol. 63, no. 11, pp. 3917–3928, Nov. 2015.
- [28] X. Gao, F. Tufvesson, and O. Edfors, "Massive MIMO channels – measurements and models," in *Proc. Asilomar'13*, Pacific Grove, CA, 2013, pp. 280–284.
- [29] C. F. Lopez and C.-X. Wang, "Novel 3D non-stationary wideband models for massive MIMO channels," *IEEE Trans. Wireless Commun.*, vol. 17, no. 5, pp. 2893–2905, May 2018.
- [30] S. Wu, C.-X. Wang, H. Aggoune, M. M. Alwakeel, and Y. He, "A non-stationary 3D wideband twin-cluster model for 5G massive MIMO channels," *IEEE J. Sel. Areas Commun.*, vol. 32, no. 6, pp. 1207–1218, June 2014.
- [31] S. Wu, C.-X. Wang, H. Haas, H. Aggoune, M. M. Alwakeel, and B. Ai, "A non-stationary wideband channel model for massive MIMO communication systems," *IEEE Trans. Wireless Commun.*, vol. 14, no. 3, pp. 1434–1446, Mar. 2015.
- [32] S. Wu, C.-X. Wang, H. Aggoune, M. M. Alwakeel, and X. You, "A general 3D non-stationary 5G wireless channel model," *IEEE Trans. Commun.*, vol. 66, no. 7, pp. 3065–3078, July 2018.
- [33] C.-X. Wang, S. Wu, L. Bai, X. You, J. Wang, and C.-L. I, "Recent advances and future challenges for massive MIMO channel measurements and models," *Sci. China Inf. Sci.*, Invited Paper, vol. 59, no. 2, pp. 1–16, Feb. 2016.
- [34] A. F. Molisch, "Ultra-wide-band propagation channels," *Proc. IEEE*, vol. 97, no. 2, pp. 353–371, Feb. 2009.
- [35] K. Haneda, A. Richter, and A. F. Molisch, "Modeling the frequency dependence of ultra-wideband spatio-temporal indoor radio channels," *IEEE Trans. Antennas Propag.*, vol. 60, no. 6, pp. 2940–2950, June 2012.
- [36] Y. F. Chen and V. K. Dubey, "Dynamic simulation model of indoor wideband directional channels," *IEEE Trans. Veh. Technol.*, vol. 55, no. 2, pp. 417–430, Mar. 2006.
- [37] J. Medbo, K. Börner, and K. Haneda, et al., "Channel modelling for the fifth generation mobile communications," in *Proc. EuCAP'14*, The Hague, Netherlands, Apr. 2014, pp. 219–223.
- [38] V. Nurmela, P. Kyösti, K. Kusume, and T. Jämsä, "METIS channel models," ICT-317669-METIS, Deliverable D1.4, Feb. 2015.
- [39] M. Peter, K. Sakaguchi, and S. Jaeckel, et al., "Measurement campaigns and initial channel models for preferred suitable frequency ranges," H2020-ICT-671650-mmMAGIC/D2.1, Deliverable D2.1, Mar. 2016.
- [40] S.-K. Yong, "TG3c channel modeling subcommittee final report." IEEE 802.15-07-0584-01-003c, 2007.
- [41] A. Maltsev, A. Sadri, and R. Maslennikov, et al., "Channel models for 60 GHz WLAN systems," IEEE doc: 802.11-09/0334r8, May, 2010.
- [42] A. Maltsev, A. Pudueyev, and I. Bolotin, et al., "Channel modeling and characterization," Deliverable D5.1, June 2014.
- [43] T. S. Rappaport, S. Sun, and R. Mayzus, et al., "Millimeter wave mobile communications for 5G cellular: It will work!" *IEEE Access*, vol. 1, pp. 335–349, 2013.
- [44] C. Gustafson, K. Haneda, S. Wyne, and F. Tufvesson, "On mm-wave multipath clustering and channel modeling," *IEEE Trans. Antennas Propag.*, vol. 62, no. 3, pp. 1445–1455, Mar. 2014.
- [45] White paper on "5G Channel Model for bands up to 100 GHz," ver 2.0, Mar. 2016. Available: <http://www.5gworkshops.com/5GCM.html>
- [46] Proposal on IMT-2020 channel model. Available: https://www.itu.int/md/R15-WP5D-C-0459/_page.print
- [47] Y. Tan, C.-X. Wang, J. Ø. Nielsen, and G. F. Pedersen, "Comparison of stationarity regions for wireless channels From 2 GHz to 30 GHz," in *Proc. IWCMC'17*, Invited Paper, Valencia, Spain, June 2017.
- [48] A. Gehring, M. Steinbauer, I. Gaspard, and M. Grigat, "Empirical channel stationarity in urban environments," in *Proc. EPMCC'01*, Vienna, Austria, Feb. 2001.
- [49] Y. Tan, J. Nielsen, and G. Pedersen, "Spatial stationarity of ultrawideband and millimeter wave radio channels," *Int J Antennas Propag.*, vol. 2016, article ID 3212864, 7 pages, 2016.
- [50] J. Turkka, P. Kela, and M. Costa, "On the spatial consistency of stochastic and map-based 5G channel models," in *Proc. IEEE CSCN'16*, Berlin, Germany, 31 Oct.–2 Dec. 2016, pp. 1–7.
- [51] M. Herdin and E. Bonek, "A MIMO correlation matrix based metric for characterizing non-stationarity," in *Proc. IST Mobile Wireless Commun. Summit*, Lyon, France, Jun. 2004, 5 pages.
- [52] M. Herdin, N. Czink, H. Ozelcik, and E. Bonek, "Correlation matrix distance, a meaningful measure for evaluation of non-stationary MIMO channels," in *Proc. IEEE VTC'05-Spring*, Stockholm, Sweden, Jan. 2005, vol. 1, pp. 136–140.
- [53] O. Renaudin, V. Kolmonen, P. Vainikainen, and C. Oestges, "Impact of correlation matrix estimation accuracy on the computation of stationarity intervals," in *Proc. EuCAP'10*, Barcelona, Spain, Apr. 2010, pp. 1–5.
- [54] A. F. Molisch, "6.8.1 Appendix 6.A: Validity of WSSUS in Mobile Radio Channels," *Supplementary Material for Second Edition*, John Wiley & Sons. Available: <http://www.wiley.com/go/molisch>
- [55] W. Q. Malik, D. J. Edwards, and C. J. Stevens, "Frequency dependence of fading statistics for ultrawideband systems," *IEEE Trans. Wireless Commun.*, vol. 6, no. 3, pp. 800–804, Mar. 2007.
- [56] A. Maltsev, A. Pudueyev, R. Weiler, M. Peter, W. Keusgen, and I. Bolotin, "Virtual antenna array methodology for outdoor millimeter-wave channel measurements," in *Proc. IEEE GC'16 Workshops*, Washington, DC, 2016, pp. 1–6.
- [57] W. Q. Malik and A. F. Molisch, "Ultra-wide band antenna arrays and directional propagation channels," in *Proc. EuCAP'06*, Nice, France, Nov. 2006.
- [58] B. H. Fleury, M. Tschudin, R. Heddergott, D. Dahlhaus, and K. Ingeman Pedersen, "Channel parameter estimation in mobile radio environments using the SAGE algorithm," *IEEE J. Sel. Areas Commun.*, vol. 17, no. 3, pp. 434–450, Mar. 1999.
- [59] R. Feng, J. Huang, J. Sun, and C.-X. Wang, "A novel 3D frequency domain SAGE algorithm with applications to parameter estimation in mmWave massive MIMO indoor channels," *Sci. China Inf. Sci.*, vol. 60, no. 8, Aug. 2017.
- [60] K. Haneda, C. Gustafson, and S. Wyne, "60 GHz spatial radio transmission: multiplexing or beamforming?," *IEEE Trans. Antennas Propag.*, vol. 61, no. 11, pp. 5735–5743, Nov. 2013.
- [61] M. Pätzold, *Mobile Radio Channels, Second Edition*. John Wiley & Sons, 2011.
- [62] A.F. Molisch, K. Balakrishnan, and D. Cassioli, et al., "IEEE802.15.4a channel model subgroup final report," IEEE P802.15, pp. 943–968, 2004.
- [63] V. P. G. Jiménez, et al., "A MIMO-OFDM testbed, channel measurements, and system considerations for outdoor-indoor WiMAX," in *Proc. EURASIP'09*, pp. 1–13, Dec. 2009.
- [64] N. Czink, P. Cera, J. Salo, E. Bonek, J.-P. Nuutinen, and J. Ylitalo, "A framework for automatic clustering of parametric MIMO channel data including path powers," in *Proc. IEEE VTC'06-Fall*, Quebec, Canada, Sept. 2006, pp. 1–5.
- [65] Y. S. Yoon, L. M. Kaplan, and J. H. McClellan, "TOPS: new DOA estimator for wideband signals," *IEEE Trans. Signal Process.*, vol. 54, no. 6, pp. 1977–1989, June 2006.
- [66] J. Salmi and A. F. Molisch, "Propagation parameter estimation, modeling and measurements for ultra-wide band MIMO radar," *IEEE Trans. Antennas Propag.*, vol. 59, no. 11, pp. 4257–4267, Nov. 2011.
- [67] A. V. Oppenheim, A. S. Willsky, and S. H. Nawab. *Signals and Systems, 2nd ed.* Prentice Hall, 1, 997, 2014.
- [68] N. C. Beaulieu and C. Cheng, "Efficient Nakagami-m fading channel simulation," *IEEE Trans. Veh. Technol.*, vol. 54, no. 2, pp. 413–424, Mar. 2005.
- [69] Q. Zhu, X. Dang, D. Xu, and X. Chen, "High efficient rejection method for generating Nakagami-m sequences," *Electron. Lett.*, vol. 47, no. 19, pp. 1100–1101, Sept. 2011.



YI TAN received the M.Sc. degree in Communication Systems from Lund University, Sweden, in 2012, and the Ph.D. degree from Heriot-Watt University, U.K. in 2020. Before and after his M.Sc. studies, he worked in the industry for a few years related to embedded systems, mobile phone antenna, firmware of radio chip, and SoC/IP design. He worked as a Research Assistant in Lund University in 2010 and Aalborg University from September 2014 to June 2015. He is currently working in Nokia Solutions and Networks.



Jesper Odum Nielsen received the master's degree in electronics engineering and the Ph.D. degree from Aalborg University, Denmark, in 1994 and 1997, respectively. He is currently an Associate Professor in the Section for Antennas, Propagation and Millimetre-Wave Systems, Department of Electronic Systems, Aalborg University. His main areas of interests are within wireless radio systems in general and in particular experimental investigation of the mobile radio channel, including the influence mobile device users have on the channel. Current and past activities include MIMO channel sounding and modeling, Massive-MIMO channel measurements and analysis, over-the-air (OTA) testing of active LTE terminals, measurement and analysis of millimeter-wave channels for 5G systems.



CHENG-XIANG WANG (Fellow, IEEE) received the B.Sc. and M.Eng. degrees in communication and information systems from Shandong University, Jinan, China, in 1997 and 2000, respectively, and the Ph.D. degree in wireless communications from Aalborg University, Aalborg, Denmark, in 2004.

He was a Research Assistant with the Hamburg University of Technology, Hamburg, Germany, from 2000 to 2001, a Visiting Researcher with Siemens AG Mobile Phones, Munich, Germany, in 2004, and a Research Fellow with the University of Agder,

Grimstad, Norway, from 2001 to 2005. He has been with Heriot-Watt University, Edinburgh, U.K., since 2005, where he was promoted to a Professor in 2011. In 2018, he joined Southeast University, Nanjing, China, as a Professor. He is also a part-time Professor with Purple Mountain Laboratories, Nanjing. He has authored four books, three book chapters, and more than 410 papers in refereed journals and conference proceedings, including 24 highly cited papers. He has also delivered 22 invited keynote speeches/talks and seven tutorials in international conferences. His current research interests include wireless channel measurements and modeling, B5G wireless communication networks, and applying artificial intelligence to wireless communication networks.

Dr. Wang is a Member of the Academia Europaea (The Academy of Europe), a Fellow of the IET, an IEEE Communications Society Distinguished Lecturer in 2019 and 2020, and a Highly-Cited Researcher recognized by Clarivate Analytics in 2017-2020. He is currently an Executive Editorial Committee Member of the IEEE TRANSACTIONS ON WIRELESS COMMUNICATIONS. He has served as an Editor for nine international journals, including the IEEE TRANSACTIONS ON WIRELESS COMMUNICATIONS, from 2007 to 2009, the IEEE TRANSACTIONS ON VEHICULAR TECHNOLOGY, from 2011 to 2017, and the IEEE TRANSACTIONS ON COMMUNICATIONS, from 2015 to 2017. He was a Guest Editor of the IEEE JOURNAL ON SELECTED AREAS IN COMMUNICATIONS, Special Issue on Vehicular Communications and Networks (Lead Guest Editor), Special Issue on Spectrum and Energy Efficient Design of Wireless Communication Networks, and Special Issue on Airborne Communication Networks. He was also a Guest Editor for the IEEE TRANSACTIONS ON BIG DATA, Special Issue on Wireless Big Data, and is a Guest Editor for the IEEE TRANSACTIONS ON COGNITIVE COMMUNICATIONS AND NETWORKING, Special Issue on Intelligent Resource Management for 5G and Beyond. He has served as a TPC Member, a TPC Chair, and a General Chair for more than 80 international conferences. He received 12 Best Paper Awards from IEEE GLOBECOM 2010, IEEE ICCT 2011, ITST 2012, IEEE VTC 2013-Spring, IWCMC 2015, IWCMC 2016, IEEE/CIC ICC 2016, WPMC 2016, WOCC 2019, IWCMC 2020, and WCSP 2020. Also, he received the 2020 AI 2000 Most Influential Scholar Award Honourable Mention in recognition of his outstanding and vibrant contributions in the field of Internet of Things between 2009 and 2019.



Gert Frølund Pedersen received the B.Sc. E.E. degree (Hons.) in electrical engineering from the College of Technology, Dublin, Ireland, in 1991, and the M.Sc. E.E. and Ph.D. degrees from Aalborg University, in 1993 and 2003, respectively.

Since 1993, he has been with Aalborg University where he is a Full Professor heading the Antennas, Propagation and Millimeter-wave Systems LAB with 25 researchers. He is also the Head of the Doctoral School on wireless communication with some 40 Ph.D. students enrolled. His research interests include

radio communication for mobile terminals especially small antennas, diversity systems, propagation, and biological effects. He has published more than 500 peer reviewed papers, 6 books, 12 book chapters and holds over 50 patents. He has also worked as a Consultant for developments of more than 100 antennas for mobile terminals including the first internal antenna for mobile phones in 1994 with lowest SAR, first internal triple-band antenna in 1998 with low SAR and high TRP and TIS, and lately various multiantenna systems rated as the most efficient on the market. He has worked most of the time with joint university and industry projects and have received more than 21 M\$ in direct research funding. He is currently the Project Leader of the RANGE project with a total budget of over 8 M\$ investigating high performance centimeter/ millimeter-wave antennas for 5G mobile phones. He has been one of the pioneers in establishing over-the-air measurement systems. The measurement technique is now well established for mobile terminals with single antennas and he was chairing the various COST groups with liaison to 3GPP and CTIA for over-the-air test of MIMO terminals. He is currently involved in MIMO OTA measurement.



QIUMING ZHU received the B.S. degree in electronic engineering and the M.S. and Ph.D. degrees in communication and information systems from the Nanjing University of Aeronautics and Astronautics (NUAA), Nanjing, China, in 2002, 2005, and 2012, respectively. Since 2012, he has been an Associate Professor with the Department of Electronic and Information Engineering, NUAA. From 2016 to 2017, he was also an Academic Visitor at Heriot-Watt University. His research interests include channel modeling for the next generation mobile communication system and wireless channel simulator and emulator.